Journal of Alloys and Compounds 787 (2019) 133–139

Contents lists available at ScienceDirect

Journal of Alloys and Compounds

journal homepage: http://www.elsevier.com/locate/jalcom

In situ synthesis of monoclinic β-Ga_2O_3 nanowires on flexible substrate and solar-blind photodetector

Shunli Wang [a, 1], Hanlin Sun [a, 1], Zhe Wang [a], Xiaohui Zeng [a], Goran Ungar [a, c], Daoyou Guo [a, *], Jingqin Shen [b], Peigang Li [b, **], Aiping Liu [a], Chaorong Li [a], Weihua Tang [b]

[a] Key Laboratory of Optical Field Manipulation of Zhejiang Province & Center for Optoelectronics Materials and Devices, Department of Physics, Zhejiang Sci-Tech University Hangzhou, 310018, China
[b] State Key Laboratory of Information Photonics and Optical Communications & Information Functional Materials and Devices, School of Science, Beijing University of Posts and Telecommunications, Beijing 100876, China
[c] Department of Engineering Materials, University of Sheffield, Mappin Street, Sheffield S1 3JD, UK

ARTICLE INFO

Article history:
Received 21 December 2018
Received in revised form
30 January 2019
Accepted 3 February 2019
Available online 6 February 2019

Keywords:
β-Ga_2O_3 nanowires
Flexible
CVD
Solar-blind UV photodetector
High working temperature

ABSTRACT

Flexible solar-blind deep ultraviolet (UV) photodetectors based on β-Ga_2O_3 have important applications in wearable portable UV light monitoring and smart skins devices. However, flexible devices limit the maximum working temperature, and amorphous nature of film grown under low temperature displays instability. In this work, monoclinic β-Ga_2O_3 nanowires were synthesized *in situ* on a flexible glass fiber fabric by chemical vapor deposition with a diameter of 40–280 nm and a length of one to tens of microns under a high temperature. The fabricated photodetector based on β-Ga_2O_3 nanowires network exhibits a good solar-blind UV photoelectric performance such as an I_{light}/I_{dark} ratio of 260, a photoresponsivity of 0.71 A/W and a decay time of 0.19 s under 254 nm UV light illumination. Meanwhile, the performance of the device is not affected by bending conditions. Simple fabrication method and excellent photoelectric performance reveal that this device will be a promising candidate for future flexible solar-blind photodetectors with a high working temperature and high stability.

1. Introduction

Solar-blind ultraviolet (UV) photodetectors, with the characteristics of high sensitivity, strong anti-interference property and low false alarm rate, have a wide range of applications in military and civilian fields such as missile tracking, fire detection, secure communication, chemical/biological analysis [1–10], etc. In recent years, much effort has been devoted to various wide band gap semiconductors to design solar-blind photodetectors, such as AlGaN [11], ZnMgO [12], diamond [13] and β-Ga_2O_3 [14–16]. Among them, β-Ga_2O_3 with a direct wide band gap of 4.9 eV, without the necessity of alloying process, excellent thermal and chemical stability is considered as an ideal candidate for solar-blind photodetector [3,17–20]. So far, solar-blind photodetectors based on various forms of β-Ga_2O_3, including single crystal [21], thin films [14,22–24] and nanostructures [25–27], have been extensively studied by researchers.

In view of the development trend of modern electronic technology, flexible electronic devices, including wearable bio-integrated devices, deformable displays and paper electronic devices, play more and more significant roles in our lives [28–33]. Take the detector as an example, robust deformability and low cost promise flexible detectors have versatile applications in portable electronic gadgets and display devices as well as biomedical imaging [34]. Recently, flexible photodetectors based on amorphous Ga_2O_3 have been reported [34–36]. Cui et al. reported that amorphous Ga_2O_3 solar-blind photodetectors were successfully manufactured on rigid quartz and flexible polyethylene naphthalate (PEN) substrates at room temperature. The results revealed that flexible devices have compatible performance with the rigid ones, and no significant degradation was observed during bending and fatigue tests [34]. Lee et al. achieved the growth of ultrathin (3–50 nm) amorphous gallium oxide films on a polyimide substrate by low-temperature (<250 °C) atomic layer deposition and examined the performance of flexible deep UV photodetectors. The flexible photodetector yielded a high level of signal-to-noise ratio

* Corresponding author.
** Corresponding author.
E-mail addresses: dyguo@zstu.edu.cn (D. Guo), pgli@zstu.edu.cn (P. Li).
[1] These authors contributed equally to this work.

https://doi.org/10.1016/j.jallcom.2019.02.031
0925-8388/

under deep UV illumination. The dark current was as low as 0.7 pA at −10 V, and the photocurrent increased significantly with enhancement factors (I_{253nm}/I_{dark}) of approximately 8×10^3 under deep UV illumination [36].

However, the device displays an instability nature due to the amorphous film grown on flexible substrates under low temperature. In addition, flexible devices put limitations on the maximum working temperatures since plastic substrates generally have low glass transition temperatures of 80–150 °C [34]. As a result, it can not work properly in a high temperature. Therefore, it is essential to explore a flexible substrate that can be applied to high temperatures for high-quality flexible Ga_2O_3 solar-blind photodetectors.

In this work, monoclinic β-Ga_2O_3 nanowires were prepared *in situ* on a flexible substrate at high temperature for the first time by the chemical vapor deposition (CVD) technique using a glass fiber fabric as substrate. As a new type of flexible substrate, glass fiber fabrics exhibit some unique properties such as high temperature resistance, non-flammable, high strength and chemical corrosion resistance [37]. This high silica glass fiber fabric model is TS-BXB with a specification of 0.06 MM × 1.20 M, which maintains its physicochemical properties at 1000 °C. The metal-semiconductor-metal (MSM) structure solar-blind UV photodetector based on β-Ga_2O_3 nanowire network exhibits a good solar-blind UV photoresponse. In addition, the performance of the device exhibits no obvious degradation in bending tests. Simple fabrication method and excellent photoelectric performance demonstrate that the device has great potential applications in the future.

2. Experimental

2.1. In situ synthesis of β-Ga_2O_3 nanowires

β-Ga_2O_3 nanowires were synthesized *in situ* by the CVD technique. Firstly, the glass fiber fabric substrates were ultrasonically cleaned by alcohol, ethanol and distilled water for 10 min, respectively, and then dried in a vacuum oven for 12 h at 60 °C. A thin film of Au (~10 nm) was deposited on the substrates under a vacuum of 10^{-4} Pa by radio frequency magnetron sputtering technique. Then the liquid metal Ga (25 mg) was coated evenly on the surface of Au-substrates (10×10 mm^2) using polydimethylsiloxane (PDMS) film at a heating plate (T = 60 °C). After that, the Ga/Au-coated samples were placed in a horizontal tube furnace, and the tube was evacuated by a mechanical rotary pump, purged with 500 sccm of argon. Then the furnace temperature was raised to 900 °C at a rate of ~30 °C/min with introducing mixture of high-purity nitrogen and oxygen gas (flow ratio of 10:1) into the chamber. After reaction for 2–10 h, the furnace was cooled down to room temperature naturally, and white fluffy products were observed on the substrate. Detailed reaction process is shown in Fig. 1(a).

2.2. Characterization of β-Ga_2O_3 nanowires

The crystalline structure of samples were analyzed by a Bruker D8 DISCOVER X-ray diffractometer (XRD). The ultraviolet–visible (UV–vis) absorption spectrum were taken using a Hitachi U-3900 UV–vis spectrophotometer. The surface morphology of β-Ga_2O_3 nanowires were characterized by a Hitachi S-4800 field-emission scanning electron microscope (SEM) equipped with an energy dispersive spectrum (EDS) and a JEOL JEM-2100 transmission electron microscopy (TEM).

2.3. Fabrication and characterization of the UV photodetector

In order to investigate the solar-blind UV photoelectric property of β-Ga_2O_3 nanowires, the MSM structure network photodetectors were constructed, and the schematic illustration was shown in Fig. 1(b). Two drops of Ag mixed paste were patterned on the as-synthesized samples and dried at 60 °C as two metal electrodes. Each electrode area was about 0.25 mm^2 and the gap between two electrodes was approximately 5 mm, which was connected to the electrodes through two copper wires for electrical measurement. The current-voltage (*I-V*) characteristics and time-dependent photoresponse of the UV photodetector was investigated by a semiconductor characterization system (Keithley-4200) equipped with a 7 W lamp as the light source of 254 nm and 365 nm.

3. Results and discussion

Fig. 2(a) shows the XRD patterns of β-Ga_2O_3 nanowires prepared at 900 °C for 5 h. All diffraction peaks in the patterns can be easily indexed according to JCPDS (Card No. 43–1012) for β-Ga_2O_3 with monoclinic structure, with the lattice constants of a = 12.23 Å, b = 3.04 Å, c = 5.80 Å, $\alpha = 90°$, $\gamma = 90°$ and $\beta = 103.7°$ [38]. It is noticed here that no other crystalline phase of Ga_2O_3 are observed in our XRD results, indicating that the synthesized product is a high-purity single-phase β-Ga_2O_3.

Fig. 2(b) shows the UV–vis absorbance spectrum of β-Ga_2O_3 nanowires prepared at 900 °C for 5 h. Obviously, β-Ga_2O_3 nanowires have a significant absorption at wavelengths less than 250 nm, near the lower edge of the solar-blind region. The optical band gap is measured by extrapolating the linear region of the plot $(\alpha h\nu)^2$ *versus* $h\nu$ and taking the intercept on the $h\nu$-axis [3,39]. The

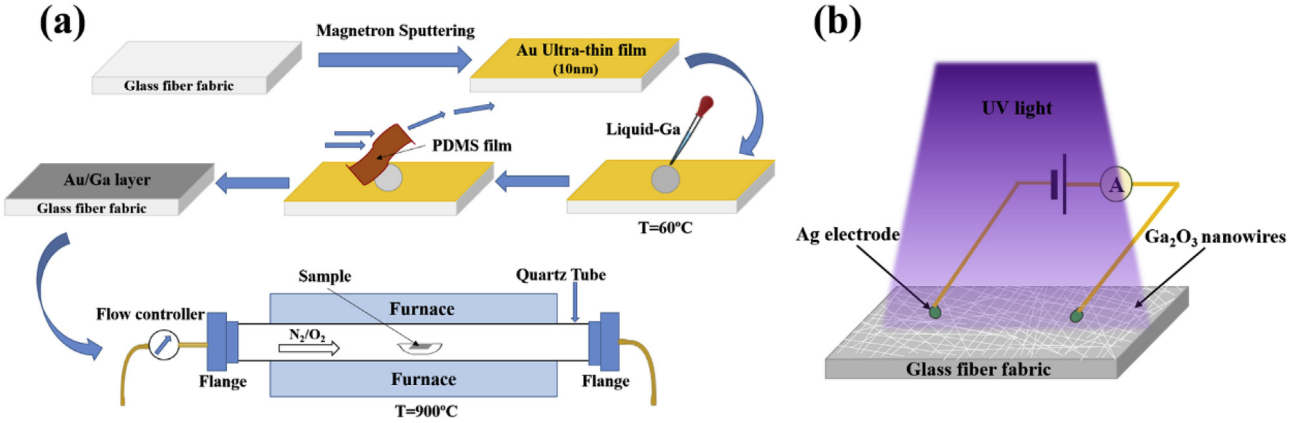

Fig. 1. (a) The schematic diagram of synthesis of β-Ga_2O_3 nanowires. (b) The schematic of the fabrication of β-Ga_2O_3 nanowires network photodetector.

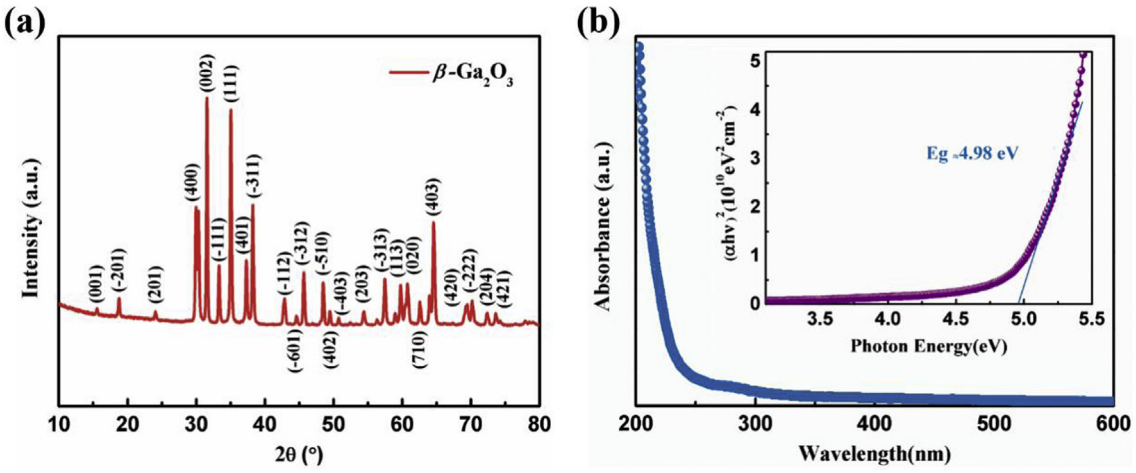

Fig. 2. (a) XRD patterns of β-Ga_2O_3 nanowires. (b) UV–vis absorption spectra of β-Ga_2O_3 nanowires with the plot of $(\alpha h\nu)^2$ *versus* $h\nu$ in the inset.

band gap of β-Ga_2O_3 nanowires is estimated to be ~4.98 eV as shown in the inset of Fig. 2(b), which is similar to the band gap of reported by others [14].

Fig. 3(a–d) presents plain-view SEM images of β-Ga_2O_3 nanowires at various times. The SEM results show that a large area of intertwined β-Ga_2O_3 nanowires were formed on the substrate. The diameter of the nanowires generally ranges from 40 to 280 nm and length from one to tens of micrometers. A larger diameter of nanowires will be obtained with a longer growth time, which can be confirmed by partial magnification SEM images of nanowires

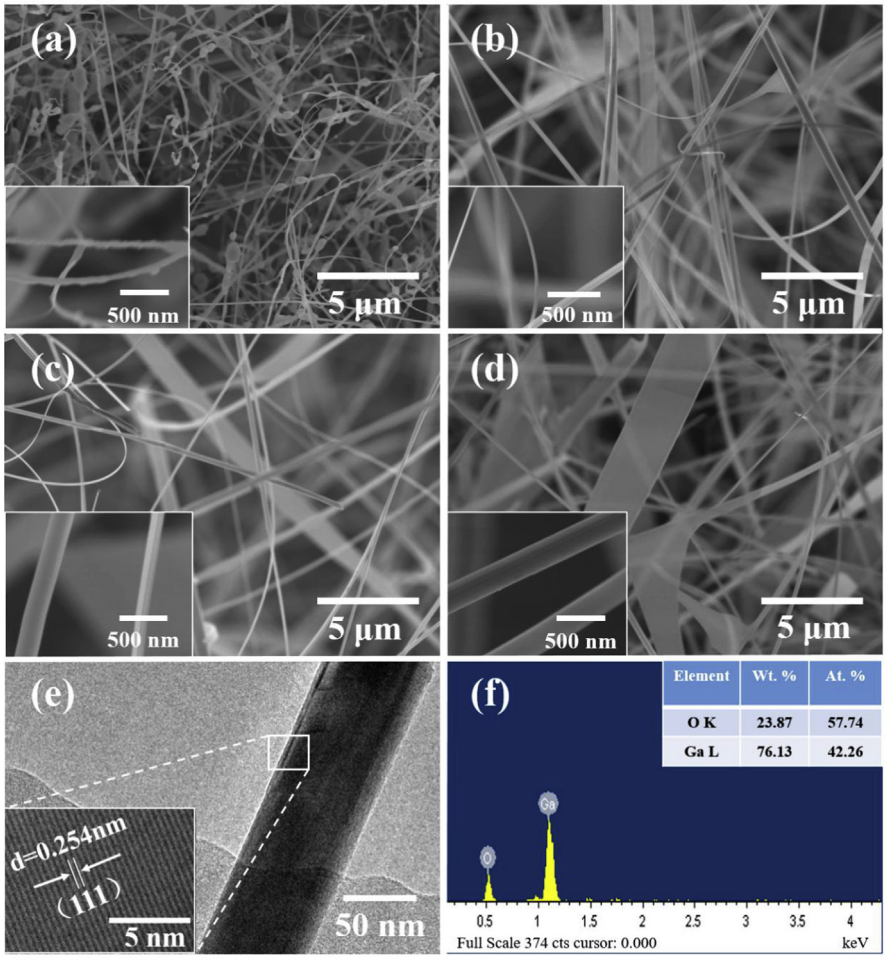

Fig. 3. SEM images of β-Ga_2O_3 nanowires prepared at different times of (a) 2 h, (b) 5 h, (c) 8 h, and (d) 10 h, and the insets are corresponding partial enlargements. (e) Low- and high-resolution (inset) TEM images of a single β-Ga_2O_3 nanowire. (f) EDS of (b).

(inset pictures of Fig. 3(a–d)).

β-Ga_2O_3 nanowires are grown via the well-developed vapor phase technique, which is based on the reaction between Ga vapor and oxygen gas [40,41]. The governing mechanisms are vapor–liquid–solid and vapor–solid (VLS and VS). Generally, the VLS mechanism determines the growth direction and diameter of nanowires, while the radial growth is involved in the VS process [42]. Nanowires will thicken due to the radial growth mechanism. Here, we propose that the growth mechanism of our nanowires is dominated by a combination of VLS and VS. When the time is lower, the preferential growth orientation is along the axial direction due to VLS mechanism and the growth at the sidewall of the nanowires is much suppressed. With increasing of grown time, a small amount of nanobelt structures growing along the side wall can be found. This phenomenon is attributed to the supersaturated vapor pressure of the gas phase material exceeding the equilibrium state of the side wall, which is the VS mechanism.

A typical low-resolution TEM image was grown at 900 °C for 5 h, as presented in Fig. 3(e), which shows a nanowire with a diameter of about 80 nm. And the high-resolution TEM image is also shown in the inset of Fig. 3(e). The lattice fringes with a d-spacing of 0.254 nm were observed, which correspond to the (111) lattice planes of β-Ga_2O_3. The EDS of nanowires grown at 900 °C for 5 h is shown in Fig. 3(f). It can be clearly shown that the resulting nanowires are mainly composed of Ga and O atoms in a ratio of about 2:3, and no other detectable elements are found.

Fig. 4(a) shows *I-V* characteristics of the fabricated photodetector in dark, under 365 nm light, and under 254 nm light with the linear and logarithmic (inset) coordinate. It is worth noting that the dark current of the device is about 8.4 nA when the bias is 20 V. The *I-V* curve measured under 365 nm light does not show an obvious increase as compared to the *I-V* curve in dark, which suggests the β-Ga_2O_3 thin films are not sensitive to 365 nm light. This is attributed to the large band gap of β-Ga_2O_3, in which electrons cannot jump from the valence band to the conduction band under the excitation of 365 nm light. In contrast, when the device is exposed to 254 nm light, the current shows a sharp jump, exhibiting a strong photoresponse characteristic [14]. The current increases to 2.18 μA, with a photo-to-dark current ($I_{254\ nm}/I_{dark}$) ratio of about 260. The above results show that the device has good solar-blind photoelectric properties.

Response time is another important metric to assess the capability of photodetectors. The fitting equation of the rise and decay time of the photoresponse has been reported in the previous work of our group [1,3,43]. As is shown in Fig. 4(b), for 254 nm illumination with the light intensity of 1500 μW/cm^2 at 20 V, the rise time components τ_{r1} and τ_{r2} are estimated to be 0.37 s and 4.56 s, respectively, corresponding to the fast-response component and the slow-response component of the current rise process, while the decay process has only one fast response component τ_d of approximately 0.19 s. In general, the fast-response component can be attributed to a rapid change in carrier concentration once the lamp is turned on/off, while the slow-response component is caused by carrier trapping/release due to the presence of defects such as oxygen vacancies [2,43].

Fig. 4(c) shows the effect of applied biases on the time-dependent photoresponses of the device under 254 nm light (light intensity of 1500 μW/cm^2) illumination by on/off switching. With the increase of applied bias 5, 10, 15, 20 and 25 V, the photocurrent increases to 0.17, 0.89, 1.68, 2.44 and 3.39 μA, respectively. The higher biases help to separate photogenerated electron-holes pairs, resulting in higher photo-currents [17]. After multiple illumination cycles the device still exhibits a nearly identical response, indicating the high robustness and good reproducibility of the photodetector.

In addition to the above-mentioned photoelectric response time, photodetectors also have some key performance indicators such as sensitivity, responsivity (R_λ), and external quantum efficiency (*EQE*) [1,3]. The sensitivity of the photodetector, defined as $(I_{il}\text{-}I_d)/I_d$ in percent (I_{il} and I_d are photocurrent and dark current, respectively), R_λ defined as the photocurrent generated per unit power of incident light on the effective area of a photoconductor, and *EQE* defined as the number of electrons detected per incident photon. The larger their values, the better the performance of the device. R_λ and *EQE* can be expressed in the following equations: $R_\lambda = I_p/(PS)$ and $EQE = hcR_\lambda/(e\lambda)$ Where $I_p = I_{il}$ - I_d, where P is the incident light intensity, S is the effective area of the photodetector, h is the Planck's constant, c is the velocity of light, e is the electronic charge, and λ is the incident light wavelength. In our systems, when the light intensity is 1500 μW/cm^2, the R_λ and *EQE* values increase as the applied bias increases [Fig. 4(d)]. The maximum R_λ and *EQE* obtained at 25 V are 0.71 A/W and 246.6%, respectively, with a sensitivity of 238.6.

To assess the effect of light intensity on the performance of the device, 254 nm light with intensity ranging from 200 to 1200 μW/cm^2 was irradiated on the photodetector at 20 V, as shown in Fig. 4(e). With the increase of the light intensity, the photocurrent increases. Fig. 4(f) presents the photocurrent as a function of light intensity. It's obvious that the photocurrent increases linearly with the increase of the light intensity. Higher light intensities excite more photogenerated electron-hole pairs, resulting in higher photocurrents [17,43].

To investigate the bending influence on photoresponse characteristics of photodetectors, the *I-V* characteristics and time response were performed on device under different bending conditions. Here, a schematic diagram of the device in a flat and bending conditions is shown in the inset of Fig. 5(a). The curved device is considered to be on the circumference of radius *r*, the value of which means the degree of curvature. Fig. 5(a) and (b) show *I-V* characteristics and time-dependent photoresponse of device at flat and different bending radius r_1,r_2 and r_3 ($r_1 = 12$ mm, $r_2 = 10$ mm, $r_3 = 8$ mm). The device under bending conditions all exhibit almost the same performance as in the flat state. Negligible differences in these curves can be attributed to the different contact conditions between the probe and the electrode when the device is bent, which indicates that the device will have a wide application prospect in the field of flexible optoelectronics.

The relationship between diameter and photoconductivity of nanowires is briefly discussed, which is helpful in improving the performance of future research photodetectors. The band-bending produced by nanowire surface states is an important factor that results into enhancement of photoconductivity of nanowires based photodetectors [44]. Due to the large surface-to-volume ratio, nanowires contain an extremely high density of surface states. Nanowires exhibit a depletion space charge layer due to the pinning of the Fermi energy at the surface, which provides physical separation of electrons and holes, resulting in a significant increase in photogenerated carrier lifetime (persistent photoconductivity) [44]. Since the carrier distribution inside the nanowire is mainly determined by the surface potential and Fermi energy pinning, which largely depends on the geometry of the wire. The dark and light currents in the nanowires vary greatly with its size [45]. The related literature on theoretical calculations of nanowires has shown that small diameters (minimal band bending) result in full depletion of the nanowires, thus minimize the dark current. Large diameters (appreciable band bending) increase the

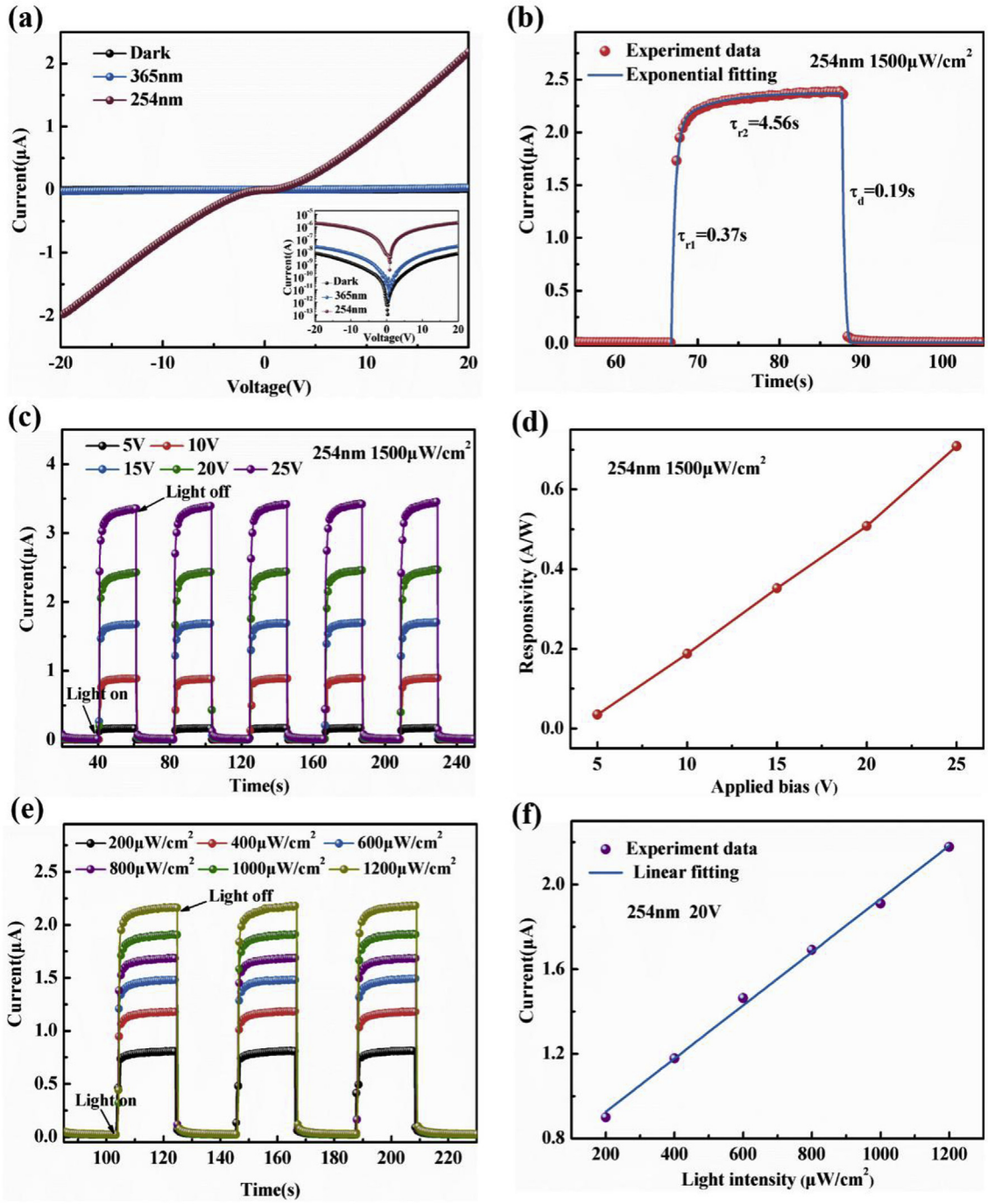

Fig. 4. (a) *I-V* characteristics curve of the photodetector with the linear and logarithmic (inset) coordinate in dark, under 365 nm light, and under 254 nm light. (b) Experimental curve and fitted curve of the photocurrent rise and decay process to 254 nm light illumination. (c) Time-dependent photoresponse of the photodetector to 254 nm light illumination by on/off switching under varied applied bias. (d) R_λ of the photodetector under varied applied bias. (e) Time-dependent photoresponse of the photodetector to 254 nm light illumination by on/off switching with varied light intensity. (f) Photocurrent as a function of the light intensity.

photoconductivity by hindering photogenerated carrier recombination [46].

4. Conclusions

In summary, we have successfully synthesized β-Ga_2O_3 nanowires *in situ* on the flexible glass fiber fabric substrates by CVD technique. Depending on the growth time, the nanowires have a diameter of about 40–280 nm and a length of one to tens of microns. The solar-blind UV photodetector based on β-Ga_2O_3 nanowire network exhibits good solar-blind UV photoresponse. Meanwhile, the photodetector exhibits the high robustness and good reproducibility, achieving varying degrees of bending without affecting its performance. Simple fabrication method and excellent photoelectric performance demonstrated that this photodetector will have great potential application in the future flexible solar-blind photodetectors with a high working temperature and high stability.

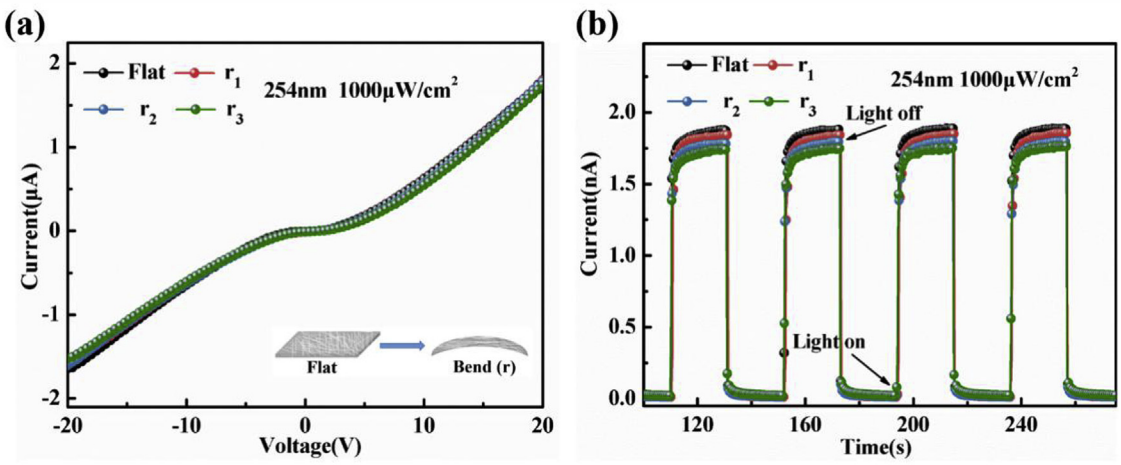

Fig. 5. (a) *I-V* characteristics and (b) time-dependent photoresponse of device (under 254 nm light illumination) at flat and different bending radius. The inset of (a) shows a schematic diagram of the device in a flat and bending conditions.

Acknowledgements

This work was supported by the National Natural Science Foundation of China (No. 61704153, 51572241, 61774019, 51572033), Zhejiang Public Service Technology Research Program/Analytical Test (LGC19F040001), Open Fund of IPOC (BUPT), Science and Technology Department of Zhejiang Province Foundation (No. 2017C37017), Scientific Research Project for the Education Department of Zhejiang Province (No. Y201738294).

References

[1] D. Guo, Y. Su, H. Shi, P. Li, N. Zhao, J. Ye, S. Wang, A. Liu, Z. Chen, C. Li, Self-Powered ultraviolet photodetector with super high photoresponsivity (3.05 A/W) based on the GaN/Sn:Ga_2O_3 pn junction, ACS Nano 12 (2018) 12827–12835.
[2] P. Li, H. Shi, K. Chen, D. Guo, W. Cui, Y. Zhi, S. Wang, Z. Wu, Z. Chen, W. Tang, Construction of GaN/Ga_2O_3 p-n junction for an extremely high responsivity self-powered UV photodetector, J. Mater. Chem. C 5 (2017) 10562–10570.
[3] D. Guo, H. Liu, P. Li, Z. Wu, S. Wang, C. Cui, C. Li, W. Tang, Zero-power-consumption solar-blind photodetector based on β-Ga_2O_3/NSTO heterojunction, ACS Appl. Mater. Interfaces 9 (2017) 1619–1628.
[4] J. Xu, W. Yang, H. Chen, L. Zheng, M. Hu, Y. Li, X. Fang, Efficiency enhancement of TiO_2 self-powered UV photodetectors using transparent Ag nanowires electrode, J. Mater. Chem. C 6 (2018) 3334–3340.
[5] Y. Chen, Y. Lu, C. Lin, Y. Tian, C. Gao, L. Dong, C. Shan, Self-Powered diamond/β-Ga_2O_3 photodetectors for solar-blind imaging, J. Mater. Chem. C (2018) 5727–5732.
[6] J. Han, D. Zhang, G. Cheng, L. Guo, J. Ren, Object detection in optical remote sensing images based on weakly supervised learning and high-level feature learning, IEEE T. Geosci. Remote. 53 (2015) 3325–3337.
[7] W. Zhong, W. Tu, S. Feng, A. Xu, Photocatalytic H_2 evolution on CdS nanoparticles by loading FeSe nanorods as co-catalyst under visible light irradiation, J. Alloy. Comp. 772 (2019) 669–674.
[8] W. Zhong, S. Shen, S. Feng, Z. Lin, Z. Wang, B. Fang, Facile fabrication of alveolate $Cu_{2-x}Se$ microsheets as a new visible-light photocatalyst for discoloration of Rhodamine B, CrystEngComm 20 (2018) 7851–7856.
[9] H. Yang, L. Geng, Y. Zhang, G. Chang, Z. Zhang, X. Liu, M. Lei, Y. He, Graphene-templated synthesis of palladium nanoplates as novel electrocatalyst for direct methanol fuel cell, Appl. Surf. Sci. 466 (2019) 385–392.
[10] X. Wang, Y. Cui, T. Li, M. Lei, J. Li, Z. Wei, Recent advances in the functional 2D photonic and optoelectronic devices, Adv. Opt. Mater. (2018), 1801274.
[11] G. Bao, D. Li, X. Sun, M. Jiang, Z. Li, H. Song, H. Jiang, Y. Chen, G. Miao, Z. Zhang, Enhanced spectral response of an AlGaN-based solar-blind ultraviolet photodetector with Al nanoparticles, Optic Express 22 (2014) 24286–24293.
[12] X. Chen, K.W. Liu, X. Wang, B.H. Li, Z. Zhang, X. Xie, D. Shen, Performance enhancement of ZnMgO film UV photodetector by HF solution treatment, J. Mater. Chem. C 5 (2017) 10645–10651.
[13] E.V. Gorokhov, A.N. Magunov, V.S. Feshchenko, A.A. Altukhov, Solar-blind UV flame detector based on natural diamond, Instrum. Exp. Tech. 51 (2008) 280–283.
[14] D. Guo, Z. Wu, P. Li, Y. An, H. Liu, X. Guo, H. Yan, G. Wang, C. Sun, L. Li, Fabrication of β-Ga_2O_3 thin films and solar-blind photodetectors by laser MBE technology, Opt. Mater. Express 4 (2014) 1067–1076.
[15] W. Kong, G. Wu, K. Wang, T. Zhang, Y. Zou, D. Wang, L. Luo, Graphene-β-Ga_2O_3 heterojunction for highly sensitive deep UV photodetector application, Adv. Mater. 28 (2016) 10725–10731.
[16] S. Luan, L. Dong, R. Jia, Analysis of the structural, anisotropic elastic and electronic properties of β-Ga_2O_3 with various pressures, J. Cryst. Growth 505 (2019) 74–81.
[17] D.Y. Guo, Z.P. Wu, Y.H. An, X.C. Guo, X.L. Chu, C.L. Sun, L.H. Li, P.G. Li, W.H. Tang, Oxygen vacancy tuned Ohmic-Schottky conversion for enhanced performance in β-Ga_2O_3 solar-blind ultraviolet photodetectors, Appl. Phys. Lett. 105 (2014), 023507.
[18] B. Zhao, F. Wang, H. Chen, Y. Wang, M. Jiang, X. Fang, D. Zhao, Solar-blind avalanche photodetector based on single ZnO-Ga_2O_3 core-shell microwire, Nano Lett. 15 (2015) 3988.
[19] S. Oh, C.K. Kim, J. Kim, High responsivity β-Ga_2O_3 metal-semiconductor-metal solar-blind photodetectors with ultraviolet transparent graphene electrodes, ACS Photonics 5 (2017) 1123–1128.
[20] L. Dong, R. Jia, C. Li, B. Xin, Y. Zhang, Ab initio study of N-doped β-Ga_2O_3 with intrinsic defects: the structural, electronic and optical properties, J. Alloy. Comp. 712 (2017) 379–385.
[21] C. Yang, H. Liang, Z. Zhang, X. Xia, P. Tao, Y. Chen, H. Zhang, R. Shen, Y. Luo, G. Du, Self-powered SBD solar-blind photodetector fabricated on the single crystal of β-Ga_2O_3, RSC Adv. 8 (2018) 6341–6345.
[22] K. Arora, N. Goel, M. Kumar, M. Kumar, Ultra-high-performance of self-powered β-Ga_2O_3 thin film solar-blind photodetector grown on cost-effective Si substrate using high-temperature seed layer, ACS Photonics 6 (2018) 2391–2401.
[23] Y. Xu, Z. An, L. Zhang, Q. Feng, J. Zhang, C. Zhang, Y. Hao, Solar blind deep ultraviolet β-Ga_2O_3 photodetectors grown on sapphire by the Mist-CVD method, Opt. Mater. Express 8 (2018) 2941–2947.
[24] L. Dong, R. Jia, B. Xin, B. Peng, Y. Zhang, Effects of oxygen vacancies on the structural and optical properties of β-Ga_2O_3, Sci. Rep. 7 (2017) 40160.
[25] X. Chen, K. Liu, Z. Zhang, C. Wang, B. Li, H. Zhao, D. Zhao, D. Shen, Self-powered solar-blind photodetector with fast response based on Au/β-Ga_2O_3 nanowires array film Schottky junction, ACS Appl. Mater. Interfaces 8 (2016) 4185–4191.
[26] R. Zou, Z. Zhang, Q. Liu, J. Hu, L. Sang, M. Liao, W. Zhang, High detectivity solar-blind high-temperature deep-ultraviolet photodetector based on multi-layered (l00) facet-oriented β-Ga_2O_3 nanobelts, Small 10 (2014) 1848–1856.
[27] T. He, Y. Zhao, X. Zhang, W. Lin, K. Fu, C. Sun, F. Shi, X. Ding, G. Yu, K. Zhang, Solar-blind ultraviolet photodetector based on graphene/vertical Ga_2O_3 nanowire array heterojunction, Nanophotonics 7 (2018) 1557–1562.
[28] Z. Zhu, D. Ju, Y. Zou, Y. Dong, L. Luo, T. Zhang, D. Shan, H. Zeng, Boosting fiber-shaped photodetectors via “soft” interfaces, ACS Appl. Mater. Interfaces 9 (2017) 12092–12099.
[29] K. Liu, M. Sakurai, M. Aono, Enhancing the humidity sensitivity of Ga_2O_3/SnO_2 core/shell microribbon by applying mechanical strain and its application as a flexible strain sensor, Small 8 (2012) 3599–3604.
[30] A. Manekkathodi, M.Y. Lu, C.W. Wang, L.J. Chen, Direct growth of aligned zinc oxide nanorods on paper substrates for low-cost flexible electronics, Adv. Mater. 22 (2010) 4059–4063.
[31] Z. Wang, H. Wang, B. Liu, W. Qiu, J. Zhang, S. Ran, H. Huang, J. Xu, H. Han, D. Chen, Transferable and flexible nanorod-assembled TiO_2 cloths for dye-sensitized solar cells, photodetectors, and photocatalysts, ACS Nano 5 (2011) 8412–8419.
[32] S. Lin, X. Bai, H. Wang, H. Wang, J. Song, K. Huang, C. Wang, N. Wang, B. Li, M. Lei, H. Wu, Roll-to-Roll production of transparent silver-nanofiber-

network electrodes for flexible electrochromic smart windows, Adv. Mater. 29 (2017), 1703238.
[33] G. Cheng, P. Zhou, J. Han, Learning rotation-invariant convolutional neural networks for object detection in VHR optical remote sensing images, IEEE T. Geosci. Remote. 54 (2016) 7405–7415.
[34] S. Cui, Z. Mei, Y. Zhang, H. Liang, X. Du, Room-temperature fabricated amorphous Ga_2O_3 high-response-speed solar-blind photodetector on rigid and flexible substrates, Adv. Opt. Mater. 5 (2017), 1700454.
[35] H. Zhuang, J. Yan, C. Xu, D. Meng, Transparent conductive Ga_2O_3/Cu/ITO multilayer films prepared on flexible substrates at room temperature, Appl. Surf. Sci. 307 (2014) 241–245.
[36] S.H. Lee, S.B. Kim, Y.-J. Moon, S.M. Kim, H.J. Jung, M.S. Seo, K.M. Lee, S.-K. Kim, S.W. Lee, High-responsivity deep-ultraviolet-selective photodetectors using ultrathin gallium oxide films, ACS Photonics 4 (2017) 2937–2943.
[37] S. Zhang, J. Cao, Y. Shang, L. Wang, X. He, J. Li, P. Zhao, Y. Wang, Nanocomposite polymer membrane derived from nano TiO_2-PMMA and glass fiber nonwoven: high thermal endurance and cycle stability in lithium ion battery applications, J. Mater. Chem. A 3 (2015) 17697–17703.
[38] J. Li, X. Chen, Z. Qiao, M. He, H. Li, Large-scale synthesis of single-crystalline β-Ga_2O_3 nanoribbons, nanosheets and nanowires, J. Phys. Condens. Matter 13 (2001) L937.
[39] Q. Liu, D. Guo, K. Chen, Y. Su, S. Wang, P. Li, W. Tang, Stabilizing the metastable γ phase in Ga_2O_3 thin films by Cu doping, J. Alloy. Comp. 731 (2018) 1225–1229.
[40] J.Y. Li, Z.Y. Qiao, X.L. Chen, L. Chen, Y.G. Cao, M. He, H. Li, Z.M. Cao, Z. Zhang, Synthesis of β-Ga_2O_3 nanorods, J. Alloy. Comp. 306 (2000) 300–302.
[41] J. Du, J. Xing, C. Ge, H. Liu, P. Liu, H. Hao, J. Dong, Z. Zheng, H. Gao, Highly sensitive and ultrafast deep UV photodetector based on a β-Ga_2O_3 nanowire network grown by CVD, J. Phys. D Appl. Phys. 49 (2016), 425105.
[42] X.L. Chen, Y.C. Lan, J.Y. Li, Y.G. Cao, M. He, Radial growth dynamics of nanowires, J. Cryst. Growth 222 (2001) 586–590.
[43] K. Chen, C. He, D. Guo, S. Wang, Z. Chen, J. Shen, P. Li, W. Tang, Low-voltage-worked photodetector based on Cu_2O/GaOOH shell-core heterojunction nanorod arrays, J. Alloy. Comp. 755 (2018) 199–205.
[44] S. Kumar, S. Dhara, R. Agarwal, R. Singh, Study of photoconduction properties of CVD grown β-Ga_2O_3 nanowires, J. Alloy. Comp. 683 (2016) 143–148.
[45] C. Soci, A. Zhang, X.Y. Bao, H. Kim, Y. Lo, D. Wang, Nanowire photodetectors, J. Nanosci. Nanotechnol. 10 (2010) 1430–1449.
[46] R. Calarco, M. Marso, T. Richter, A.I. Aykanat, R. Meijers, V.D.H. A, T. Stoica, H. Lüth, Size-dependent photoconductivity in MBE-grown GaN-nanowires, Nano Lett. 5 (2005) 981.

Update

Journal of Alloys and Compounds

Volume 807, Issue , 30 October 2019, Page

DOI: https://doi.org/10.1016/j.jallcom.2019.151768

Journal of Alloys and Compounds 807 (2019) 151768

Contents lists available at ScienceDirect

Journal of Alloys and Compounds

journal homepage: http://www.elsevier.com/locate/jalcom

Corrigendum

Corrigendum to "*In situ* synthesis of monoclinic β-Ga_2O_3 nanowires on flexible substrate and solar-blind photodetector" [J. Alloy. Comp. 787 (2019) 133–139]

Shunli Wang [a, 1], Hanlin Sun [a, 1], Zhe Wang [a], Xiaohui Zeng [a], Goran Ungar [a, c], Daoyou Guo [a, *], Jingqin Shen [b], Peigang Li [b, **], Aiping Liu [a], Chaorong Li [a], Weihua Tang [b]

[a] *Key Laboratory of Optical Field Manipulation of Zhejiang Province & Center for Optoelectronics Materials and Devices, Department of Physics, Zhejiang Sci-Tech University Hangzhou, 310018, China*

[b] *State Key Laboratory of Information Photonics and Optical Communications & Information Functional Materials and Devices, School of Science, Beijing University of Posts and Telecommunications, Beijing, 100876, China*

[c] *Department of Engineering Materials, University of Sheffield, Mappin Street, Sheffield, S1 3JD, UK*

We regret for that there is an error in the original manuscript. We made corrections, as listed below.

Page 138. "Fig. 5. (b) Time-dependent photoresponse of the device (under 254 nm light illumination) at flat and different bend radii." The y-coordinate in this figure should be "**μA**" instead of "**nA**".

The corrected Fig. 5. is shown below.

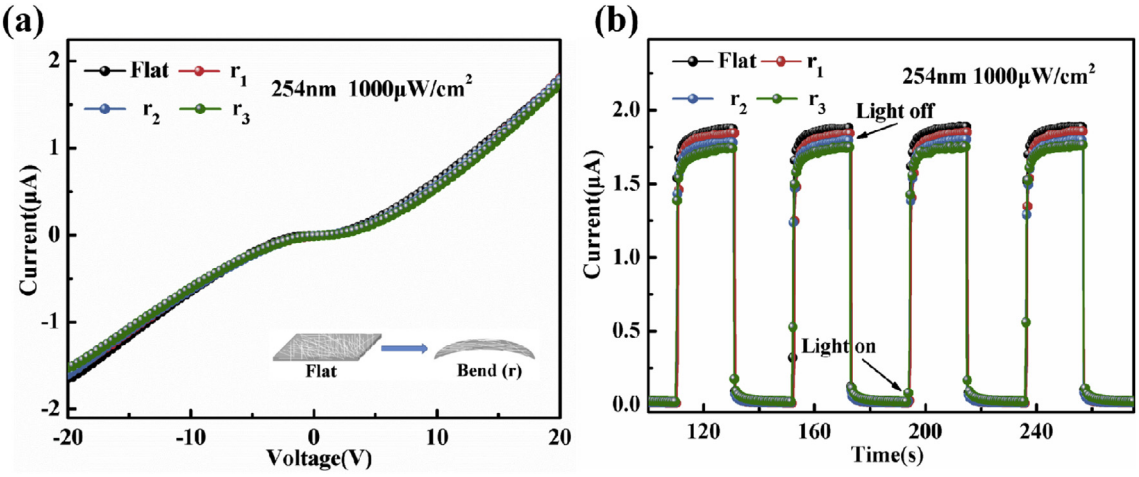

We feel quite sorry for the mistake and the trouble bringing to your work.

DOI of original article: https://doi.org/10.1016/j.jallcom.2019.02.031.

* Corresponding author.

** Corresponding author.

E-mail addresses: dyguo@zstu.edu.cn (D. Guo), pgli@zstu.edu.cn (P. Li).

[1] These authors contributed equally to this work.

https://doi.org/10.1016/j.jallcom.2019.151768